Annals of Nuclear Energy 223 (2025) 111657

Contents lists available at ScienceDirect

Annals of Nuclear Energy

journal homepage: www.elsevier.com/locate/anucene

Evaluation of the transmutation capability of TRU and MA in a 700 MWt molten chloride salt fast reactor

Yoshihisa Tahara [a,*], Chikako Ishizuka [b], Haruka Hirano [b]

[a] NAIS Co. Inc., 416 Muramatsu, Tokai-mura, Naka-gun, Ibaraki 319-1112, Japan
[b] Institute of Science Tokyo, N1-16, 2-12-1, Ookayama, Meguro-ku, Tokyo 152-8550, Japan

ARTICLE INFO

Keywords:
Molten salt reactor
Fast reactor
Chloride salt
Transmutation
Transuranic element
Minor actinide

ABSTRACT

The transmutation capability of transuranic elements (TRU) and minor actinides (MA) for a small 700 MWt molten chloride salt fast reactor (MCSFR) has been evaluated based on burnup calculations using spent fuel from PWRs and compared with that of a sodium-cooled fast reactor (SFR). Burnup calculations were performed using the online reprocessing capability of the Serpent 2 code.

This MCSFR is a loop type reactor, and the molten fuel salt circulates through the core and the loops outside the core. An effective neutron flux, corrected using the times for fuel to transit the core and the loops, was introduced into the burnup equation to account for such a fuel circulation.

After almost 10 years of burnup calculation, it has been found that the MCSFR has a TRU transmutation capability equivalent to that of an SFR with a conversion ratio of 0.5 and that the MA transmutation capability increases with the amount of MA loading and becomes higher than that of an SFR. Although MCSFR requires about twice as much loading fuel as its core, it has inherent safety features, allows for more efficient fuel utilization, and greatly reduces MA.

1. Introduction

After the 2011 Fukushima nuclear accident, utilizing the existing light water reactors was promoted, although high safety was required. However, the use of nuclear power stagnated for more than 10 years after the accident, especially in Japan (Nuclear Power 10 Years After Fukushim, 2021; Fukushima nuclear accident). In recent years, the momentum for nuclear power generation as a base load power source has been gathering in coexistence with renewable energy sources, intending to become carbon–neutral. Under these circumstances, sodium-cooled fast reactors (SFR) and high-temperature gas-cooled reactors (HTGR) have been selected as future nuclear power systems in Japan, and research is being promoted (White paper 2024).

Looking back at the Fukushima accident, it is necessary that, in any accident, a reactor settles safely at a low power level, and the decay heat can be removed. The molten salt reactor is indeed such a reactor with a high degree of self-control (Mochizuki 2024), and although there are many issues to be solved from the point of view of Technology Readiness Levels (Gougar et al., 2015): corrosion effects, the integrity of metallic materials, fuel salt physical properties, nuclear material safeguards, licensing consideration, and so on, it is a promising reactor type, and research is being promoted worldwide.

To utilize natural resources effectively, the nuclear fuel materials in the spent fuel discharged from the LWRs must be burned efficiently. From a geological disposal point of view, reducing MA as high-level radioactive waste by transmuting is one useful way. Fast reactors are suitable for these purposes because the number of neutrons emitted per fission is large in the fast energy region.

In a fast reactor of thorium-molten salt using fluoride (LiF), a large amount of Pu and MA has been reported to be incinerated (Li 2024). However, in this study, to avoid radioactive tritium production through reactions ^{6}Li(n, t)^{4}He and ^{7}Li(n, tn')^{4}He and to make the neutron spectrum harder than fluoride (Holcomb et al., 2011), molten chloride salts are used. It is also reported that in a molten chloride-salt fast reactor whose initial loading fuel has a spent fuel composition of BWR, a conversion ratio of 1.0 can be achieved by using chlorine-37 enriched to 100 %, and power generation can be continued by feeding only depleted uranium (Mitachi 2022).

Against this background, the purpose of this study is to clarify the transmutation capability of TRU and MA of MCSFR with natural chlorine and to show that MCSFR is effective in terms of utilizing natural resources and reducing MA and is worth developing as a future energy

* Corresponding author at: 416 Muramatsu, Tokai-mura, Naka-gun, Ibaraki 319-1112, Japan.
E-mail address: tahara@nais.ne.jp (Y. Tahara).

https://doi.org/10.1016/j.anucene.2025.111657
Received 14 March 2025; Received in revised form 30 April 2025; Accepted 12 June 2025
Available online 26 June 2025

supply system.

Chapter 2 describes the burnup analysis model of MCSFR with external loops. Chapter 3 provides the fuel composition and other data used in this analysis. Chapter 4 shows the results of the burnup calculations. Chapter 5 discusses the flow of the MCSFR operation. Chapter 6 presents the conclusions obtained.

2. Analysis model

2.1. Calculation method

In criticality analysis, Serpent 2 (Leppänen et al., 2015), a continuous-energy Monte Carlo computer code developed by VTT (Technical Research Center of Finland), was used. The ACE nuclear data file (NEA JEFF-3.3) based on JEFF-3.3 (Plompen et al., 2020) was used as cross-section data for the criticality calculation. In addition, the fission yield and decay data files included in the JEFF-3.3 release were used for the burnup calculation. The parameters for the simulated neutron population in criticality source mode are 20,000 neutrons per batch, 560 batches, and 60 skip batches for a total of 10 million neutron histories. In the burnup calculation, one step was 2 months (60 days), and one year was 6 steps (360 days), for a burnup of about 10 years (3600 days). The Serpent code features a function for continuous online reprocessing. This function supplies fuel nuclides to maintain the core in a critical state while removing fission products (FPs) from the core. To activate this function in Serpent 2, the following input cards should be used: 'rep' defines reprocessor: mode 0 for feeding fuel and mode 1 for transferring FPs to storage tanks; 'mat' defines material; 'mflow' defines the material flow; 'dep pro' links a reprocessor to the depletion calculation.

2.2. Burnup model

In the case of solid fuel, where the fuel is in a static state, the change in nuclides in the fuel is described by the well-known burnup equation. However, the influence caused by external loops has to be incorporated into the burnup equation for a molten salt reactor where fuel is circulated through the core and external loops.

Let us consider a molten salt reactor in Fig. 1, consisting of a core and external loops. There are no structural components or control rods within the core.

It was assumed that mixing occurs within the core, and a uniform composition is established. Therefore, the feeding fuel injected into the core is immediately mixed uniformly within the core, which contributes to maintaining criticality. The nuclides burn continuously in the core under a neutron flux corresponding to 700 MWt. The loss of reactivity due to burnup is compensated by feeding fuel and discharging FPs.

The sum of the amount lost by nuclear reaction that occurs when fuel passes through the core and the amount lost due to radioactive decay during circulation through the core and the external loops is compensated by feeding fresh fuel into the core.

Imagine that a small portion of fuel, for example, a thin disk of fuel, ascends from the bottom to the top of the core in a transit time, τ_c. During the period, neglecting the fission reaction for simplicity, the nuclei within the portion are transmuted via the neutron capture reaction and radioactive decay. At the top of the core, the fuel portion is divided equally and flows into each external loop. The nuclei in the loops undergo radioactive decay while they circulate and enter the core again. Therefore, the loss of fuel nuclides must be compensated by feeding fuel to maintain the core critical. This requirement at the steady state is expressed in the following equation, using the fuel transit time in the external loop, τ_ℓ,

$$N(\sigma_c\phi+\lambda_\beta)\tau_c + N\lambda_\beta\tau_\ell = \lambda^{feed}N^{feed}(\tau_c+\tau_\ell). \tag{1}$$

The relationship between the critical concentration N and the fuel feeding rate λ^{feed} can be obtained from this equation as

$$N = \frac{\lambda^{feed}N^{feed}(\tau_c+\tau_\ell)}{\sigma_c\phi\tau_c+\lambda_\beta(\tau_c+\tau_\ell)} = \frac{\lambda^{feed}N^{feed}}{\sigma_c\left[\frac{\tau_c}{\tau_c+\tau_\ell}\right]\phi+\lambda_\beta}, \tag{2}$$

and the corresponding differential equation becomes

$$\frac{dN}{dt} = -N\sigma_c\left(\frac{\tau_c}{\tau_c+\tau_\ell}\phi\right) - \lambda_\beta N + \lambda^{feed}N^{feed}, \tag{3}$$

and this nuclide depletion equation can be solved.

Therefore, the influence caused by the external loops can be incorporated into the ordinary burnup equation by introducing the effective neutron flux defined below using the transit times of the core and external loops in the primary system.

$$\phi_{eff} = \frac{\tau_c}{\tau_c+\tau_\ell}\phi. \tag{4}$$

The critical fuel nuclide concentration N and the neutron flux ϕ are obtained by solving the neutron transport equation for the core geometry, and thus, the fuel feeding rate λ^{feed} is determined and vice versa.

If the fuel is in a static state, the production-destruction equation for nuclide i can be expressed by the well-known equation below, including the fission reaction and the production of FPs.

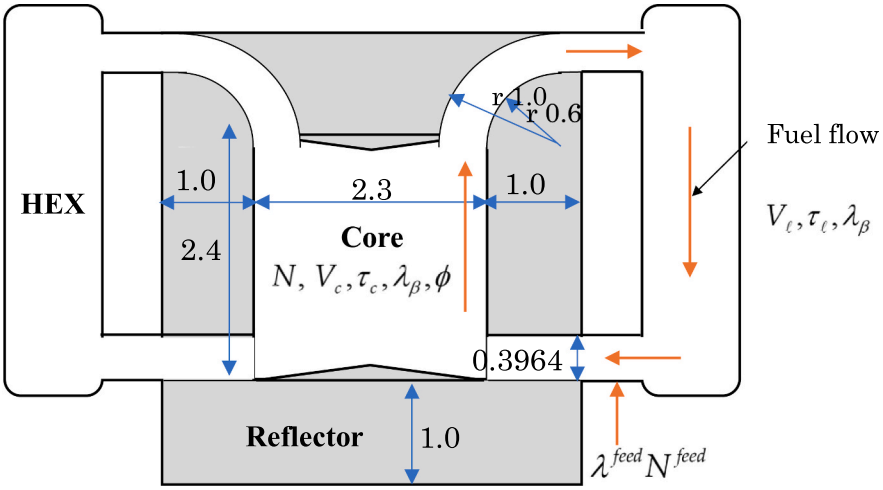

Fig. 1. Schematic diagram of MCSFR with four external loops, each having a heat exchanger (unit in meters).

$$\frac{dN_i(t)}{dt} = \left[\sum_{j=1}^{M} \ell_{ij}\lambda_j N_j + \sum_{k=1}^{M} f_{ik}\left(N_k\sigma_{c,k}\right)\phi + Y_i\Sigma_f\phi - \left(\lambda_i + \sigma_{a,i}\phi\right)N_i \right], \quad (5)$$

where on the right-hand side,

First term: Production of nuclide i by the decay of other nuclides,

Second term: Production of nuclide i by neutron capture,

Third term: Production of nuclide i by fission,

Fourth term: Destruction of nuclide i by decay and absorption.

Two modifications need to be made to Eq. (5) for a molten salt reactor. The first is to replace the flux with the effective neutron flux to consider the influence of fuel circulation. The second is to introduce fictitious decay constants: fuel feeding rate λ_i^{feed} and FPs removal rate λ_i^{repro}, which is λ_i^{D-FP} for dissolved FPs or $\lambda_i^{nonD-FP}$ for non-dissolved FPs. Thus, Eq. (5) becomes:

$$\frac{d}{dt}N_i(t) = \left\{ \sum_{j=1}^{M} \ell_{ij}\lambda_j N_j + \sum_{k=1}^{M} f_{ik}\left(N_k\sigma_{c,k}\right)\phi_{eff} + Y_i\Sigma_f\phi_{eff} - \left\{\lambda_i + \sigma_{a,i}\phi_{eff}\right\}N_i \right\} - \lambda_i^{repro}N_i + \lambda_i^{feed}N_i^{feed}. \quad (6)$$

Since the neutron flux is normalized to the core power, the effective neutron flux is calculated inside a computer code by specifying the rated power multiplied by the factor mentioned earlier as the effective core power,

$$P_{eff} = \frac{\tau_c}{\tau_c + \tau_\ell} P_{Rated\ Power}. \quad (7)$$

In addition, the molten salt density was fixed to the core average density at the rated power to maintain the core conditions at the rated power.

In the reactor operation, each heavy nuclide in the feed fuel is added to the core at the same rate, thus $\lambda_i^{feed} = \nu^{fuel}/V_{core}$; ν^{fuel} is the charge rate of feed fuel, and V_{core} is the core volume. The removal rate of the soluble FP nuclides was also set at the same rate as the feed fuel. The fuel feed rate λ^{feed} was determined through a trial-and-error process so that the effective multiplication factor k_{eff} of the core becomes approximately 1.0 during the burnup period.

The Cm isotopes are produced mainly by successive neutron capture reactions starting from ^{242}Cm produced by β^--decay of ^{242g}Am as seen in the burnup chain (Okumura et al., 2007). Therefore, an appropriate branching ratio for the neutron capture reaction of ^{241}Am should be applied to accurately evaluate the amount of Cm isotopes.

Since the default value of the branching ratio of Serpent 2 has been calculated in the PWR neutron spectrum, the branching ratio γ for MCSFR having a hard neutron spectrum was calculated by the following equation:

$$\left\langle \gamma_{(n,\gamma)}^{^{241}Am \rightarrow\ ^{242g}Am} \right\rangle = \frac{\sum_g \gamma_{(n,\gamma),g}^{^{241}Am \rightarrow\ ^{242g}Am} \sigma_{(n,\gamma),g}^{^{241}Am} \phi_g}{\sum_g \sigma_{(n,\gamma),g}^{^{241}Am} \phi_g}, \quad (8)$$

using ENDF/B-VIII.0 data (MF = 9, MT = 102) (Default isomeric branching ratios; Okumura et al., 2013; Brown et al., 2018). A value of 0.851 was obtained and applied to the burnup calculations with Serpent 2. That is lower than the default value of 0.919.

2.3. Removal of fission products

The continuous removal of FPs reduces neutron poisons and the overall radiotoxicity of the reactor inventory and improves fuel utilization, economics, safety, nuclear transmutation rate, and waste management in MSRs. The dissolved and non-dissolved FPs are handled separately. Dissolved FPs, including lanthanide nuclides, are removed by chemical reprocessing. These elements are Zn, Ga, Ge, As, Se, Br, Rb, Sr, Y, Zr, Cd, In, Sn, I, Cs, Ba, La, Ce, Pr, Nd, Pm, Sm, Eu, Gd, Tb, Dy, Ho, Er, Tm, and Yb. The removal rate of these elements was set to the same rate as the fuel feeding rate. On the other hand, all of the non-dissolved FPs, including the noble gases and noble metals, are removed by helium bubbling. The corresponding elements are H, N, O, He, Ne, Ar, Kr, Xe, Rn, Nb, Mo, Tc, Sb, Te, Lu, Hf, Ta, W, Re, Au, Ag, Pt, Pd, Rh, Ir, Ru, and Os. The removal time was set to 30 seconds (λ = 0.3333) (Frima 2013; Aufiero et al., 2013; Aufiero 2014).

2.4. Transmutation capability evaluation

Nuclear transmutation is caused by nuclear reactions (neutron capture, fission, and so on) and radioactive decay. The nuclear transmutation weight for each nuclide is evaluated through the mass balance in the operation at rated power. The weight of nuclide i is obtained by the number density of the nuclide multiplied by the volume of the primary system (the sum of the volume of the core and the total volume of the four external loops, each with a heat exchanger) as

$$W_i = N_i \times V_{primary} \times AM_i \times f = N_i \times \left(V_{core} + V_{loop}\right) \times AM_i \times f\ (ton), \quad (9)$$

where AM_i is the atomic mass of nuclide i, and f is the mass conversion factor (1amu = 1.6605 × 10^{-30} ton).

The transmutation weight (TW_j) for each element j is calculated by the following equation using the initial loading weight (IW_j), the fuel feed weight (FW_j) supplied to keep the core critical during operation, and the residual weight in the core (RW_j) at the end of operation:

$$TW_j = \left(IW_j + FW_j\right) - RW_j. \quad (10)$$

The fuel feed weight (FW_j) can be obtained by correcting the decay of ^{241}Pu and the production of ^{241}Am to the difference between the initial loading weight and the residual weight at the end of the operation when operated at 0 % rated power. The correction due to other nuclides was negligible compared to the ^{241}Pu correction.

The transmutation rate of element j (TR_j) is defined as the ratio of the transmutation weight to the sum of the initial loading weight and the fuel feed weight:

$$TR_j = \frac{TW_j}{IW_j + FW_j} \times 100\ (\%). \quad (11)$$

Normalized transmutation weight (NTW_j) is also defined as the transmutation weight divided by thermal output and operation period:

$$NTW_j = \frac{TW_j}{Q \times T_{op}} \left(\frac{g}{MW_t \cdot d}\ or \frac{kg}{GW_t \cdot y} \right). \quad (12)$$

This expresses the transmutation weight per unit of energy and time.

3. Data and conditions for analysis

(a) Composition of the molten fuel salt:

The following composition of the molten fuel salt was used,

$$35NaCl + 35CaCl_2 + (30 - x)UCl_3 + xTRUCl_3$$

where the TRU concentration x is less than 30 in mol% due to the limitation to avoid sedimentation.

(b) Density of molten fuel salt:

The density of the salt mixture was evaluated based on the recommended formulation (Mochizuki 2022; McMurray et al., 2018) using measured data (Janz et al., 1968; Monreal and Jackson, 2020). The resulting dependence of the salt density on temperature is

$$\rho(T) = 4382.7 - 0.89562 \times T(K)\ [kg/m^3]$$

From this equation, the density of molten fuel salt is 3.5990 (g/cm^3) at an average salt temperature of 875 K, and this value was used in nuclide number density calculations.

(c) Composition of PWR spent fuel:

The PWR UO_2 fuel with an enrichment of 3.9 wt% (H/U: 4.3) and the

discharge burnup of 45 GWd/t with a cooling time of 10 years (Ando and Takano, 1999) was used in this study. The weight fraction of the heavy elements and the isotopic composition are given in Table 1 and Table 2, respectively.

(d) Composition of reflector material.

The reflective material is SUS 316L, which has chlorinated stress corrosion cracking resistance and is made of ultra-low carbon steel SUS316 with intergranular corrosion resistance. The composition of the material was determined using the standards (Japanese Steels and Alloys), as shown in Table 3.

(e) Reflector temperature.

The reflector temperature was set at 875 K, equal to the average temperature of the fuel salt within the core.

(f) Density of the reflector.

The density of SUS316L at 20 ℃ is 7.98 (g/cm^3), and using the average linear expansion coefficient, the density at 875 K was calculated to be 7.73 (g/cm^3) (Physical properties of stainless steel).

(g) Volume and Transit time of fuel.

The volume of the core and the total volume of the external loops including heat exchangers are 9.7 m^3 and 11.4 m^3, respectively, and thus the volume of the primary system is 21.1 m^3. Fuel's transit time in the core is 2.46 s, and in the external loop, it is 2.69 s (Mochizuki 2022).

(h) Reactor geometry.

The reactor shown in Fig. 1 was modeled as depicted in Fig. 2 for nuclear calculations. The reactor consists of a cylindrical core and a stainless steel reflector. The diameter and height of the core are 2.3 m and 2.4 m, respectively. The reflector thickness surrounding the core is 1.0 m. The upper and lower reflectors are conical and extend 10 cm into the core, thus facilitating the rectification of the molten salt flow. Since the albedo of the reflector saturates around 60 cm thick, the results obtained in this study are considered to hold even with a reflector thickness of 60 cm from a core design point of view, and downsizing is possible.

4. Results

4.1. Neutron spectrum

The neutron spectrum of a reactor core directly relates to the nuclear characteristics of the core (criticality, reactivity coefficient, transmutation, etc.). Thus, the neutron spectra of MCSFR and SFR have been compared. The neutron spectrum (energy-dependent flux) was tallied using the Serpent 2 detector function. The neutron spectrum of MSCFR was calculated using the core model in Fig. 2. Regarding SFR, the Japanese fast reactor Monju was selected for spectrum comparison. The enrichment of MOX fuel is 23.0 and 29.9 Pu wt% for the inner and outer core, respectively (Takashita et al., 2000). Using a two- dimensional R-Z model, the neutron spectrum of the inner core region was obtained by Serpent 2. The results are shown in Fig. 3. The shape of both neutron spectra is very similar in the energy region that affects core characteristics from 10 KeV to 20 MeV. The MCSFR flux is lower than SFR at energies between 100 eV and 10 KeV but becomes higher than SFR below 100 eV.

4.2. Burnup characteristics

The burnup calculation was performed using the online reprocessing capabilities of Serpent 2. The core has an initial critical TRU concentration of 7.49 mol% and has operated for almost 10 years (3600 days). In a molten salt reactor, molten fuel salt circulates between the core and the external loops, and thus, delayed neutron precursors flow out of the core. The reactivity loss due to fuel flow is approximately 150 pcm (Tahara et al., 2024). Therefore, the critical TRU concentration was adjusted to give a k_{eff} of about 1.0150 to compensate for the reactivity loss due to fuel flow. The 25 mol% TRU fuel was continuously supplied to the core, and its feed rate was determined by trial and error to keep the core critical during operation. The burnup dependence of the effective multiplication factor and the conversion ratio is shown in Fig. 4. In the first half of the burnup period, the effective multiplication factor decreases by about 0.3 %Δk due to the accumulation of FPs, but, in the second half of the period, it has returned to approximately the initial value in part due to an increase in the conversion ratio.

The mean conversion ratio is roughly 0.6 during the operation. This is because the core lacks neutrons to raise the conversion ratio due to a large amount of absorption by the ^{35}Cl(n, p) reaction.

4.3. TRU and MA transmutation

Here, three cases are studied. In the first case, it is assumed that the reprocessed PWR spent fuel is used in the MCSFR as it is. The TRU composition is the same as the spent fuel composition of PWR described

Table 1
Weight fraction of heavy elements.

Element	U	Pu	Np	Am	Cm
Weight percent	98.71	1.130	0.06683	0.09030	0.005437

Table 2
Weight percent of heavy nuclide isotopes.

Element	Isotope				
U	^{234}U	^{235}U	^{236}U	^{238}U	
	2.1844×10^{-2}	8.8080×10^{-1}	5.3715×10^{-1}	9.8560×10^{1}	
Pu	^{238}Pu	^{239}Pu	^{240}Pu	^{241}Pu	^{242}Pu
	2.3870×10^{0}	5.5908×10^{1}	2.4916×10^{1}	9.6404×10^{0}	7.1487×10^{0}
Np	^{237}Np				
	100.00				
Am	^{241}Am	^{242m}Am	^{243}Am		
	8.0080×10^{1}	9.0087×10^{-2}	1.9830×10^{1}		
Cm	^{242}Cm	^{243}Cm	^{244}Cm	^{245}Cm	^{246}Cm
	3.6274×10^{-3}	7.9923×10^{-1}	8.8709×10^{1}	9.5031×10^{0}	9.8474×10^{-1}

Table 3
Chemical composition of SUS316L.

Element	Si	Mn	Fe	Ni	Cr	Mo
Weight percent	1	2	64	13.5	17	2.5

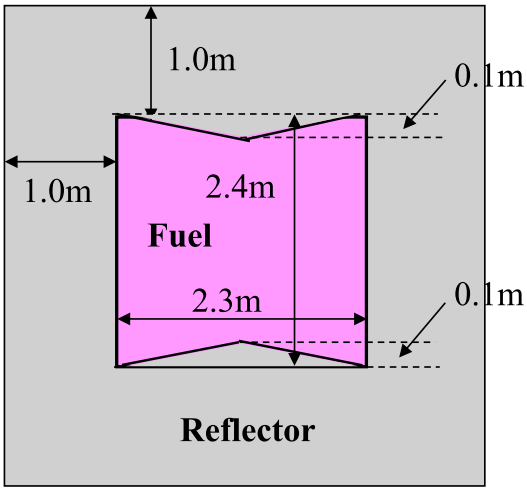

Fig. 2. Calculation model and dimensions.

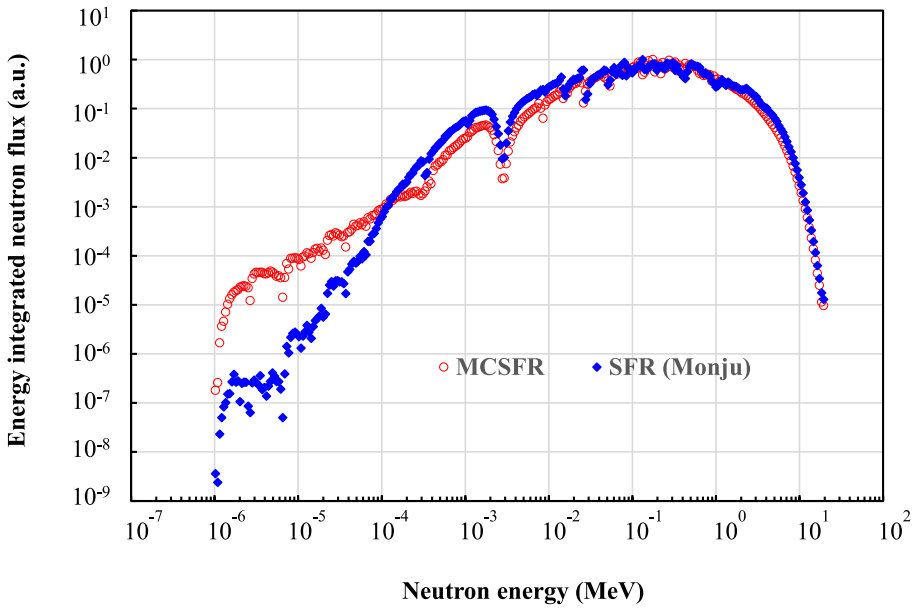

Fig. 3. Neutron spectra of MCSFR and SFR (Monju).

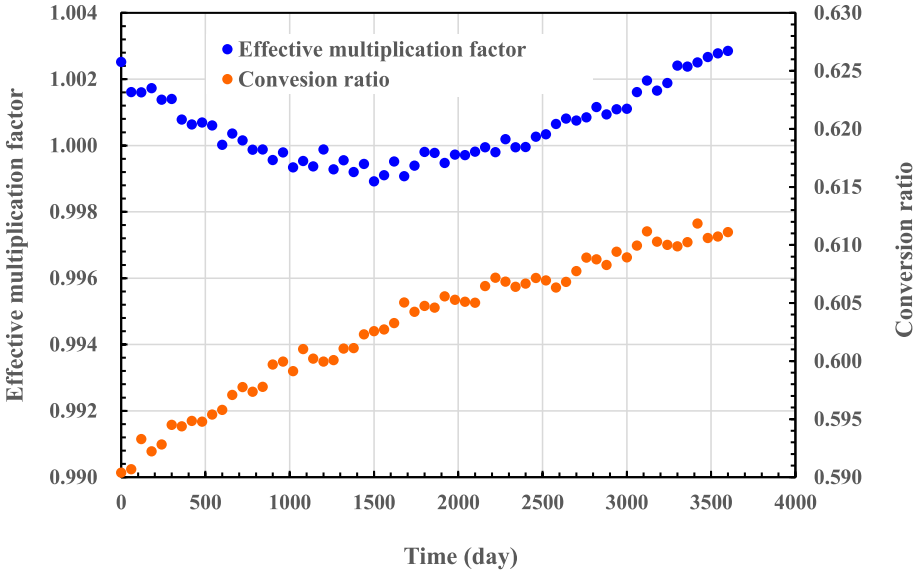

Fig. 4. Change in the effective multiplication factor and conversion ratio with time. The effective multiplication factor fluctuates around 1.001 during the operation; on the other hand, the conversion ratio increases with time, and the average is roughly 0.6.

in Table 1. The weight ratio of TRU and U was adjusted so that the core would become critical, and the concentration of TRU and MA was obtained as 7.94 mol% and 3.2 wt%, respectively. The TRU concentration of the fuel supplied during the operation was set to 25 mol%, and the charge rate of the fuel was 1.95 (L/d). The burnup characteristics of this case are described in the previous section.

The second and third cases correspond to the scenario in which MAs are separated in the PWR-spent fuel reprocessing process, mixed with Plutonium, and then transmuted in MCSFR. The composition of TRU, the weight ratio of MA to Pu, was adjusted so that the weight percentage of MA in heavy metals (U, Pu, and MA) would reach a target value of 5 or 11 wt%. Simultaneously, the concentration of TRU in mol% was also adjusted so that the core would become critical. In this way, critical TRU concentrations of 8.00 mol% and 9.98 mol% were obtained for cases with MA concentrations of 5 wt% and 11 wt%, respectively. The TRU concentration of the fuel supplied during the operation was set to 25 mol %, and the charge rate of the fuel was 1.70 (L/d) and 1.5 (L/d) for cases with MA concentrations of 5 and 11 wt%, respectively. The transmutation weight was evaluated from the change in the weight of each element during the burnup period.

4.3.1. *TRU transmutation*

The TRU transmutation capability was evaluated for the first case. The initial critical concentration of TRU in the primary system is 7.49 mol% and the Pu enrichment and the MA content in heavy metal are 21.9 wt% and 3.2 wt%, respectively. Table 4 shows the mass balance for 10 years (3600 days) of operation in the primary system (core plus external loops). The first column indicates elements contained in the system. The second column shows the initial inventory within the primary system of each chemical element. The third column represents the weight of elements supplied during the operating period, the fourth column represents the residual weight of the elements at the end of the

Table 4
Mass balance of MCSFR with 3.2 wt%MA fuel for 10 years of operation.

Elements	Initial loading* (ton)	Supply weight (ton)	Residual weight (ton)	Transmutation weight (ton)
U	25.011	0.434	23.876	1.569
Pu	7.327	1.783	8.030	1.080
MA	1.054	0.282	1.261	0.075
TRU	8.381	2.065	9.291	1.155

* The critical TRU concentration of the initial core is 7.49 mol%.

operation, and the final column represents the transmutation weight obtained by Eq. (14) using these weights.

Using the transmutation weight in Table 4, a net TRU transmutation weight normalized by the thermal output of 700 MWt is obtained as 0.46 (g/MWt-d). As recognized from Fig. 4, this value is the TRU transmutation weight for the average conversion ratio of about 0.6. On the other hand, according to Waltar et al., 2012, the TRU transmutation weight for SFR, whose conversion ratio is 0.5, is 0.47 (g/MWt-d). Therefore, the TRU transmutation capability of MCSFR is very close to that of SFR with a conversion ratio of 0.5, and it can be said that they are equivalent.

4.3.2. *MA transmutation*

The MA transmutation capability was evaluated for three cases: first, 3.2 wt%MA with the composition of the spent fuel of PWR; for this case, the mass balance is already shown in Table 4, second, 5.0 wt%MA, which is considered the upper limit for homogeneously MA loaded SFR and finally 11 wt%MA achieved in the SFR with an axially heterogeneous core with an upper sodium plenum (Fujimura et al., 2017 a). For 5.0 wt%MA, the mass balance is summarized in Table 5. This table shows that the MA transmutation weight is 33 (kg/GWt-y), which is improved but still lower than the SFR transmutation weight, and the normalized TRU transmutation weight is 0.48 (g/MWt-d).

A recent study of MA transmutation using the 'Monju' data shows that the MA transmutation weight is 212 (kg/GWe-y) at 11 wt% MA (Fujimura et al. 2017a; Fujimura et al. 2017b). The rated power of the representative core is 750 MWe/1765 MWt. This leads to a transmutation rate of 90 (kg/GWt-y), which is significantly improved over the SFR value, as shown in Table 7. This core uses the refueling scheme of 6 batches, and the MA loading is 0.649 (ton/batch) (2024 letter from Fujimura to Tahara). The transmutation rate at the discharge of a fuel batch is 40 % (Fujimura et al., 2015). Taking into account the cycle length of 19.8 months (Fujimura et al., 2017b) and the number of batches, the average transmutation rate becomes 4.0 (%/y), and the initial MA loading normalized by the thermal output power of the fuel batch becomes 2206 (kg/GWt).

The mass balance, when fuel with 11 wt% MA is loaded into MCSFR, is summarized in Table 6, and from this table, a much higher MA transmutation weight of 109 (kg/GWt-y) was obtained. In this case, the normalized TRU transmutation weight is 0.60 (g/MWt-d) from Table 6. The MA transmutation capabilities obtained so far are summarized in Table 7 for comparison. Furthermore, all results for the TRU and MA transmutation weights are shown in Fig. 5.

Table 5
Mass balance of MCSFR with 5.0 wt%MA fuel for 10 years of operation.

Elements	Initial loading* (ton)	Supply weight (ton)	Residual weight (ton)	Transmutation weight (ton)
U	24.443	0.381	23.312	1.512
Pu	7.295	1.676	7.977	0.994
MA	1.656	0.122	1.550	0.228
TRU	8.951	1.798	9.527	1.222

* The critical TRU concentration of the initial core is 8.00 mol%.

Table 6
Mass balance of MCSFR with 11.0 wt%MA fuel for 10 years of operation.

Elements	Initial loading* (ton)	Supply weight (ton)	Residual weight (ton)	Transmutation weight (ton)
U	22.239	0.338	21.325	1.252
Pu	7.490	1.386	8.114	0.762
MA	3.674	0.198	3.118	0.754
TRU	11.164	1.584	11.232	1.516

* The critical TRU concentration of the initial core is 9.98 mol%.

Table 7
Comparison of MA transmutation characteristics for cores MA loaded homogeneously.

Reactor type	MCSFR			MA transmutation SFR*	SFR**
Thermal power (MWt)	700			1765	3800
MA concentration (wt%)	3.2	5.0	11.0	11.0	5.0
Initial MA weight (kg/GWt)	1506	2366	5249	2206	695
Transmutation weight (kg/GWt-y)	11	33	109	90	53
Transmutation rate (%/y)	0.6	1.3	2.0	4.0	7.6
Transmutation efficiency (%/GWt-y)	0.8	1.9	2.8	2.3	2.0

* Fujimura et al., 2015 and 2017a, 2017b.
** Waltar et al., 2012 Fast Spectrum Reactors Table 7.12.

At 5 wt%MA, the MA transmutation weight of MCSFR is 33 (kg/GWt-y) and lower than 53 (kg/GWt-y) of SFR, but the transmutation weight (kg) is proportional to the MA inventory. Thus, it is appropriate to introduce transmutation efficiency as an index to express the potential for nuclear transmutation, which is defined as the transmutation weight (kg/GWt-y) divided by the weight (kg) of MA in the primary system. That is,

Transmutation efficiency = Transmutation weight (kg/GWt-y) / Initial weight of MA(kg) × 100 (%)

= Transmutation rate (%/y) / Rated power (GWt).

This transmutation efficiency is written in the last row of Table 7. Using this index, the transmutation capability of different types of reactors can be compared on an equal basis. In Table 7, the MA transmutation efficiency for MCSFR and SFR at 5 wt%MA is 1.9 (%/GWt-y) and 2.0 (%/GWt-y), respectively, and MCSFR and SFR are almost equivalent in the potential of nuclear transmutation of MA.

At 11 wt%MA, the MA transmutation weight is 109 (kg/GWt-y) for MCSFR and 90 (kg/GWt-y) in a recent study of SFR for MA incineration. The transmutation efficiency for them is 2.8 (%/GWt-y) and 2.3 (%/GWt-y), respectively. Therefore, MCSFR has a higher transmutation capability than the SFR of MA incineration.

The transmutation weight of MCSFR increases linearly with increasing MA concentration, as shown in Fig. 5. Thus, MCSFR can load and burn MA at high concentrations; this is a great advantage of MCSFR. However, the upper limit of the MA loading weight must be appropriately determined by a safety analysis that reflects the reactivity coefficients and reactor kinetics parameters.

4.4. *Kinetics parameters*

Kinetics parameters such as the delayed neutron fraction, decay constants of delayed neutron precursors, and the neutron generation time are important to understand how the neutron flux behaves when an accident occurs. Therefore, the dependency of these parameters on the MA concentration (wt%) was investigated.

Without MA, the effective delayed neutron fraction of MCSFR is

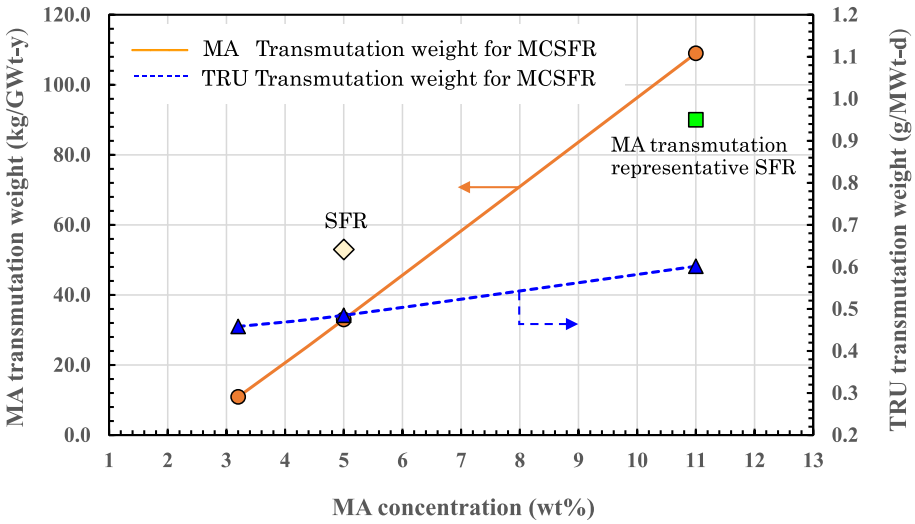

Fig. 5. Comparison of MA and TRU transmutation weights for fast reactors where minor actinides are loaded homogeneously. The circles and triangles show the MA and TRU transmutation weights of MCSFR at 3.2, 5.0, and 11 wt%, respectively. The diamond indicates the MA transmutation weight of the SFR at 5 wt% (Waltar et al., 2012). The square indicates the MA transmutation weight of the MA transmutation representative SFR at 11 wt% (Fujimura et al., 2017a,2017b).

0.396 %, and that of SFR is 0.386 % for the homogeneous 2-region oxide core and 0.391 % for the homogeneous 2-region metal core (Tachibana et al., 1990). Thus, when MA is not loaded, the delayed neutron fractions of MCSFR and SFR are almost the same.

Fig. 6 shows variations in the delayed neutron fraction and the neutron generation time versus MA concentration (wt%), and both decrease with increasing MA concentration.

The delayed neutron fraction is 0.40 % for the case without MA and decreases at a rate of 1.2 %/wt%MA with increasing MA concentration. The neutron generation time is 0.69 μs for the case without MA and decreases at a rate of 3.1 %/wt%MA with increasing MA concentration. The rate of change in neutron generation time with MA concentration is three times higher than that of the delayed neutron fraction. From this fact, in the MCSFR core design, the maximum MA concentration to be loaded must be determined by accounting for the results of transient analyses in which the kinetics parameters and reactivity coefficients of MCSFR are reflected.

5. Discussion

Summarizing the results obtained so far here. Fig. 7 shows a schematic diagram of the 700 MWt MCSFR operation and the flow of nuclear material. As a premise, a 3000 MWt PWR fueled with an enrichment of 3.9 wt%^{235}U is assumed. After 1200 days of continuous operation, the fuel batch with a burnup of 45GWd/t is discharged, cooled for 10 years, and then reprocessed. During this operation, uranium is depleted to the enrichment of 0.88 wt%^{235}U; Pu and MA are produced.

The fuel is then chlorinated and fed into the MCSFR. After 10 years of operation with online fuel reprocessing, uranium enrichment in the primary loop was reduced to 0.58 wt%, less than the natural uranium concentration of 0.71 wt%. TRU is transmuted at a rate of 0.46 g/MWt-d. This transmutation weight is equivalent to the transmutation weight of SFR with a conversion ratio of 0.5, and the transmutation weight increases with increasing MA concentration.

Regarding MA incineration, in the case of an MA concentration of 3.2 wt%, the transmutation weight is 11 (kg/GWt-y), lower than that of SFR. However, increasing MA concentration increases the MA transmutation weight, and a higher MA transmutation weight of 109 (kg/

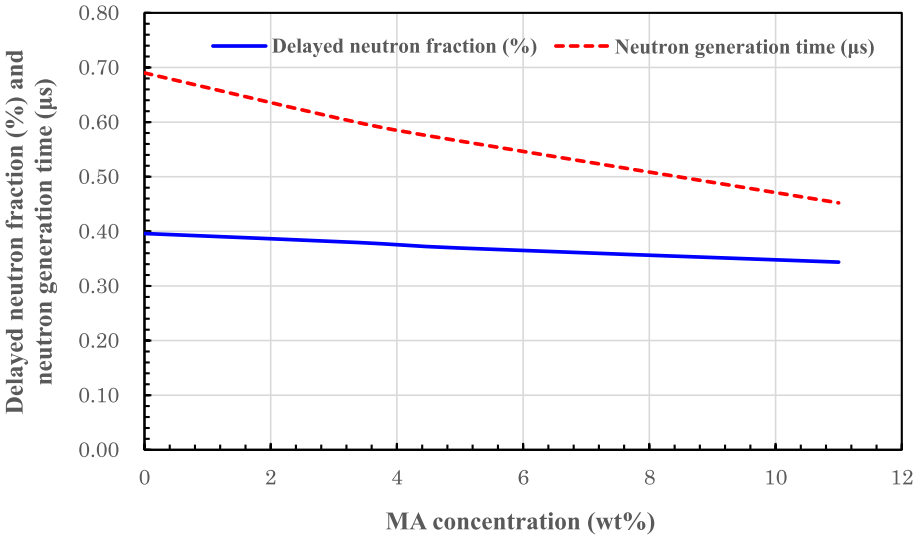

Fig. 6. Dependence of the delayed neutron fraction and the prompt neutron generation time on MA concentration.

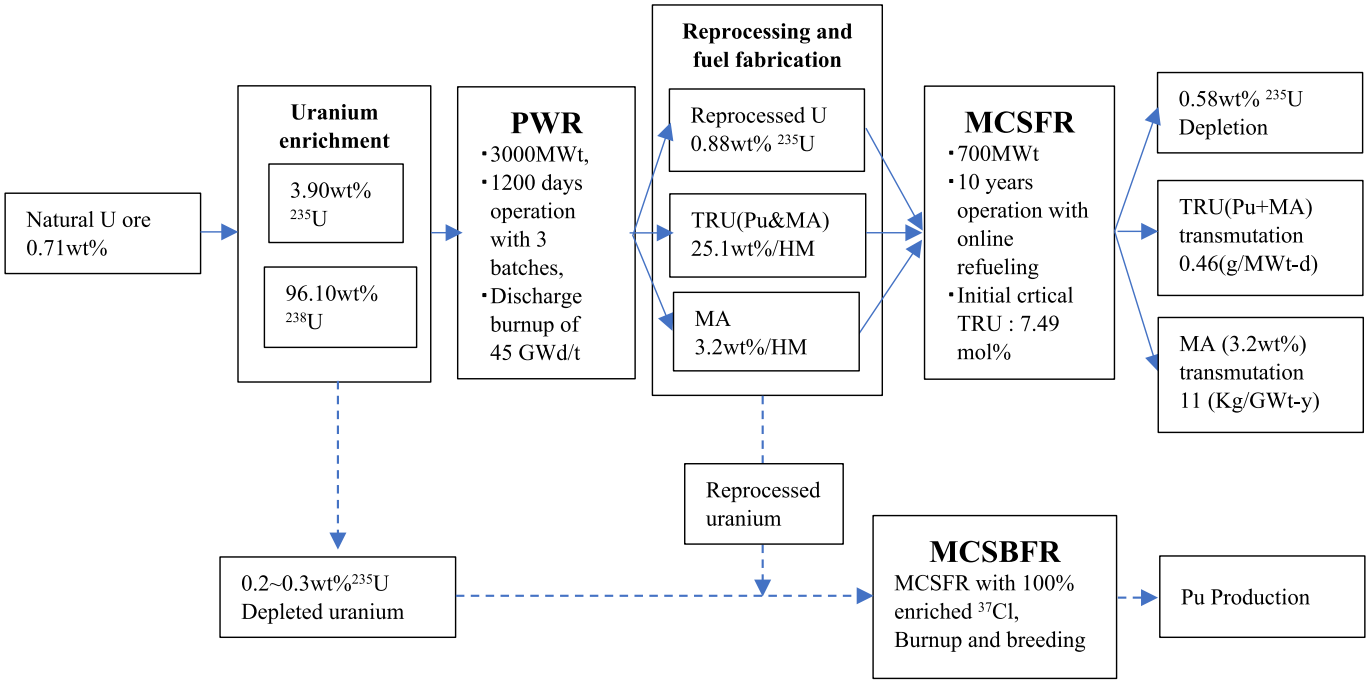

Fig. 7. Operation of a 700 MWt MCSFR and nuclear material flow.

GWt-y) than SFR is achieved at 11.0 wt%MA. Therefore, by using MCSFR and reusing spent LWR fuel (PWR fuel was assumed in this study), efficient utilization of natural uranium resources and reduction of high-level radioactive waste and radiotoxicity can be achieved.

Furthermore, by increasing the conversion ratio, for example, by using chlorine enriched to 100 % ^{37}Cl and adjusting the core size, the amount of uranium in the core, and the reprocessing rate, MCSFR becomes a breeder reactor and can continue to produce electricity and simultaneously plutonium by supplying the depleted uranium from spent fuel or uranium as residue from the uranium enrichment process (Mitachi 2022). This is shown in Fig. 7 by the dashed line.

6. Conclusions

The TRU and MA transmutation capabilities of an MCSFR of 700 MWt using fuel that has spent fuel compositions of PWR were compared with those of SFR. Conclusions are that the MCSFR is equivalent to SFR for the TRU transmutation capability and has a higher MA transmutation capability than SFR for a higher MA concentration. MCSFR features inherent safety, can use fuel efficiently, and greatly reduces MA. The details are as follows:

(a) The MCSFR can continue to operate and generate electricity by feeding molten fuel salt with the same composition as LWR spent fuel.
(b) Uranium enrichment is reduced to 0.58 wt% after almost 10 years, which is below the natural level. This demonstrates that MCSFR can use natural resources effectively.
(c) The TRU and MA transmutation weights of MCSFR increase with increasing MA concentration.
(d) MCSFR has a TRU transmutation weight of 0.46 (g/MWt-d) and is equivalent to SFR with a conversion ratio of 0.5, whose transmutation weight is 0.47 (g/MWt-d).
(e) The MA transmutation weight of MCSFR is 109 (kg/GWt-y) at an MA concentration of 11 wt% and higher than an MA transmutation SFR, whose transmutation weight is 90 (kg/GWt-y).
(f) At 5 wt%MA, the MA transmutation efficiencies for MCSFR and SFR are approximately equal to 2 (%/GWt-y), and MCSFR and SFR have equivalent MA transmutation capabilities. The MA transmutation efficiency of MCSFR increases with increasing MA concentration and 2.8 (%/GWt-y) at 11 wt%MA.
(g) The delayed neutron fraction (β_{eff}) is 0.40 % and the neutron generation time (Λ) is 0.69 μs for the case without MA. Both decrease with increasing MA concentration, and the decrease rates of β_{eff} and Λ are 1.2 %/wt%MA and 3.1 %/wt%MA, respectively. The acceptable MA concentration will be determined by considering the safety analysis results because Λ is largely dependent on the MA concentration.

Declaration of competing interest

The authors declare that they have no known competing financial interests or personal relationships that could have appeared to influence the work reported in this paper.

Acknowledgments

Part of this study was conducted as a project by the consortium led by the Beyond Energy R&D Association (BERD, Japan), which was funded by the Ministry of Economy, Trade and Industry (METI, Japan) and was commissioned by the Japan Atomic Energy Agency (JAEA) under Contract No. R05I037. The authors express sincere thanks to METI for its financial support.

The authors thank Dr. Hiroyasu Mochizuki (BERD) for managing this project and for his appropriate advice and Mr. Ritsuo Yoshioka (International Thorium Molten-Salt Forum) for information on the delayed neutron fractions of sodium-cooled fast reactors. We are also grateful to Dr. Koji Fujimura (HITACHI, Ltd.) for information on his study on the MA transmutation fast reactor and Dr. Peng Hong Liem (NAIS Co. Inc.) for his review and comments on this manuscript.

Data availability

No data was used for the research described in the article.

References

Ando Y, Takano H. Estimation of LWR spent fuel composition. Japan Atomic Energy Research Institute; 1999. (JAERI-Research 99-004). Japanese.

Aufiero, M., Cammi, A., Fiorina, C., Leppänen, J., Luzzi, L., Ricotti, M.E., 2013. An extended version of the SERPENT-2 code to investigate fuel burn-up and core material evolution of the Molten Salt Fast Reactor. J. Nucl. Mater. 2013 (441), 473 – 486.

Aufiero M, 2014. DEVELOPMENT OF ADVANCED SIMULATION TOOLS FOR CIRCULATING-FUEL NUCLEAR REACTORS [dissertation]. Milano (Italy), Politecnico di Milano: 2014.

Brown D.A., Chadwick M.B., Capote R., et al., 2018. ENDF/B-VIII.0: The 8th Major Release of the Nuclear Reaction Data Library with CIELO-project Cross Sections, New Standards and Thermal Scattering Data. Nucl. Data Sheets. 2018;148:1–142, doi:10.1016/j.nds.2018.02.001.

Default isomeric branching ratios [Internet]. Espoo (Finland): VTT [cited 2025 Mar 9]. Available from: https://serpent.vtt.fi/mediawiki/index.php?title=Default_isomeric_branching_ratios.

Frima LL, 2013. Burnup in a Molten salt fast reactor [Master Thesis]. Delft (Netherlands): Delft University of Technology;2013. NERA-131-2013-010.

Fukushima nuclear accident: Energy policy [Internet]. Wikipedia: [cited 2025 April 17]. Available from: https://en.wikipedia.org/wiki/Fukushima_nuclear_accident.

Fujimura K., Ohki S., Takeda T., 2015. Development of a Fast Reactor for Minor Actinides Transmutation, 2; Study on the MA Transmutation Core Concepts. Proceedings of Global; 2015, Sep. 20-24; Paris (France), Paper 5105.

Fujimura K., Itooka S., Ohki S., Takeda T., 2017a. Core concept of minor actinides transmutation fast reactor with improved safety. Proceedings of 2017 International Congress on Advances in Nuclear Power Plants (ICAPP 2017); 2017 April 24-28; Fukui and Kyoto (Japan), Paper 17171.

Fujimura, K., Shirakura, S., Ohki, S., Takeda, T., 2017b. Study on the Minor Actinide Transmutation utilizing Monju Data (12) MA transmutation representative reactor core. Annual meeting of AESJ; 2017. march 27-29; kanagawa (Japan), 3F01. Japanese.

Gougar HD, R. A. Bari, T. K. Kim, Sowinski TE, Worrall A, 2015. Assessment of the Technical Maturity of Generation IV Concepts for Test or Demonstration Reactor Applications, Idaho Falls (ID), Idaho National Laboratory; 2015. (INL/EXT-15-36427 Revision 2).

Holcomb DE, Flanagan GF, Patton BW, Gehin JC, Howard RL, Harrison TJ, 2011. FAST SPECTRUM MOLTEN SALT REACTOR OPTIONS, Oak Ridge (TN), ORNL;2011. (ORNL/TM-2011/105).

Janz GJ, Tomkins RPT, Allen CB, et al. Molten salts: volume 4, part 2, chloride and mixtures. Washington, D.C. 20402, USA: U.S. Department of Commerce, National Bureau of Standards; 1968.

Japanese steels and alloys [Internet]. National Technical University KhPI: Ukraine: SteelJIS [cited 2025 April 15]. Available from: http://steeljis.com/index.php.

Leppänen, J., Pusa, M., Viitanen, T., Valtavirta, V., Kaltiaisenaho, T., 2015. The Serpent monte carlo code: Status, development and applications in 2013. Ann. Nucl. Energy 2015 (82), 142–150. https://doi.org/10.1016/j.anucene.2014.08.024.

Li, D., 2024. TRU utilization and MA transmutation in thorium-based fluorinated molten salt fast reactor. Prog. Nucl. Energy 2024 (168), 105015. https://doi.org/10.1016/j.pnucene.2023.105015.

Mitachi K., 2022. Fast-Spectrum Chloride Molten Salt Reactor Having Characteristics of Fuel Self-Sufficiency. Trans. At. Energy Soc. Japan. 2022; 21(1):27-32. doi:10.3327/taesj.J21.004. Japanese.

McMurray J, Besmann T, Jerden J, et al., 2018, Multiphysics simulations for molten salt reactor evaluation: chemistry modeling and database development, ORNL/SPR-2018/864. https://info.ornl.gov/sites/publications/Files/Pub111424.pdf.

Mochizuki, H., 2022. Neutronics and thermal-hydraulics coupling analyses on transient and accident behaviors of molten chloride salt fast reactor. J. Nucl. Sci. Technol. 2131647, 1–27. https://doi.org/10.1080/00223131.2022.2131647.

Mochizuki, H., 2024. Transient behavior of a molten salt fast reactor under two-phase flow conditions with helium bubbling. Nucl. Eng. Des. 2024 (417), 1–21. https://doi.org/10.1016/j.nucengdes.2023.112825.

Monreal MJ, Jackson JM. Measuring the properties of actinide-molten salts. Technical Report. 2020. LA-UR-20–24894. United States: Los Alamos National Laboratory. doi:10.2172/1637688.

NEA: JEFF-3.3 [Internet]. Nuclear Energy Agency, [cited 2025 Mar 9]. Available from: https://www.oecd-nea.org/dbdata/jeff/jeff33/index.html.

Nuclear Power 10 Years After Fukushima: The Long Road Back [Internet]. Vienna: IAEA; 2021 [cited 2025 April 20]. Available from: https://www.iaea.org/newscenter/news/nuclear-power-10-years-after-fukushima-the-long-road-back/.

Okumura K., Kugo T., Kaneko K., Tsuchihashi K., 2007. SRAC2006: A Comprehensive Neutronics Calculation Code System. Tokai-mura (Japan). JAEA; 2007. (JAEA-Data/Code 2007-004, p.186).

Okumura K., Sugino K., Kojima K., Jin T., Okamoto T. and Katakura J., 2013. Set of ORIGEN2 Cross Section Libraries Based on JENDL-4.0: ORLIBJ40. Tokai-mura (Japan). JAEA; 2013. (JAEA-Data/Code 2012-032).

Physical properties of stainless steel [Internet]. Tokyo: Japan: JSSA [2025 April 16]. Available from: https://www.jssa.gr.jp/contents/faq-article/q6/. Japanese.

Plompen, A.J.M., Cabellos, O., De Saint, J.C., et al., 2020. The joint evaluated fission and fusion nuclear data library. JEFF-3.3. Eur Phys J A 56 (181). https://doi.org/10.1140/epja/s10050-020-00141-9.

Tachibana A., Suzuki M., Kawashima M., 1990. Nuclear static behaviors and uranium-238 fission effects in large volume cores of LMFBR. J AESJ. 1990;32(2):179-196. Japanese.

Tahara Y., Hirano H., Chiba S., Mochizuki H., Katabuchi T., 2024. Request for ^{35}Cl(n,p) reaction cross-section measurements and re-evaluations from the standpoint of molten chloride salt fast reactor design, J Nucl. Sci. Technol. 2024;61(2): 277-284. doi:10.1080/00223131.2023.2282553.

Takashita H., Higuchi M., Togashi N., Hayashi T., Report on Neutronic Design Calculation Methods (Technical Report), JNC TN8410 2000-011, May 2000.

Waltar AE, Todd DR, Tsvetkov PV, 2012, Translation from the English edition: Fast Spectrum Reactors by Alan E. Waltar, Donald R. Todd and Pavel V. Tsvetkov, Springer US 2012, Japanese translation published by arrangement with Springer-Verlag GmbH & Co KG through The English Agency (Japan) Ltd., 2016.

White paper 2024 (Annual Report on Energy), Part 3 Chapter 4 Development of nuclear energy policy [Internet]. Tokyo (Japan): Agency for Natural Resources and Energy; 2024 [cited 2025 April 20]. Available from: https://www.enecho.meti.go.jp/about/whitepaper/2024/pdf/. Japanese.